Combustion for aerospace propulsion

Destabilization of flapping sheets: The surprising analogue of soap films

H. Lhuissier [a], E. Villermaux [a,b,*]

[a] *Aix-Marseille Université, IRPHE, 13384 Marseille cedex 13, France*
[b] *Institut Universitaire de France*

Available online 22 July 2009

Abstract

When punctured, a uniform liquid sheet is known, since Taylor and Culick, to recess at a constant speed, balancing surface tension and inertia. For planar soap films, this steady solution holds until the initially smooth receding rim is violently destabilized, exhibiting deep indentations from which droplets are ejected. A surprising new three-dimensional mechanism explaining this destabilization and resulting wavelength has been demonstrated: because of the shear between the still outer medium and the receding liquid, the film flaps through a Kelvin–Helmholtz instability, itself inducing an acceleration perpendicular to the film, which intensifies with the flapping amplitude. To this acceleration is associated a classical Rayleigh–Taylor mechanism, promoting the rim indentations. *To cite this article: H. Lhuissier, E. Villermaux, C. R. Mecanique 337 (2009).*
© 2009 Published by Elsevier Masson SAS on behalf of Académie des sciences.

Keywords: Liquid films; Shear instability; Flapping; Rayleigh–Taylor instability; Atomization; Drops

1. Introduction

The transition from a compact macroscopic liquid volume to a set of dispersed smaller drops often involves as a transient stage the change of the liquid topology into a sheet shape. This transition is sometimes enforced by specific man-made devices, and also occurs spontaneously as a result of various impacts and blow-ups. An easy way to produce a spray, widely used in the context of liquid propulsion engines, is to form a liquid sheet by letting a jet impact a solid surface, or a facing alike jet (see Fig. 1).

The sheet, when the liquid is a uniform phase exempt from nucleation sites, disintegrates into drops by the desta-bilization of its edges. Pioneer works of Savart (1833) [2–4], and later Taylor (1959) [5,6] and Huang (1970) [7] essentially focused on the resulting sheet shape and its spatial extension. These depend on the impact Weber *We* formed from the ratio of the liquid inertia in a Galilean frame ρu^2 to the capillary restoring pressure σ/d where u is the velocity difference of the liquid stream with its surroundings, ρ its density, σ its surface tension and d some injection size
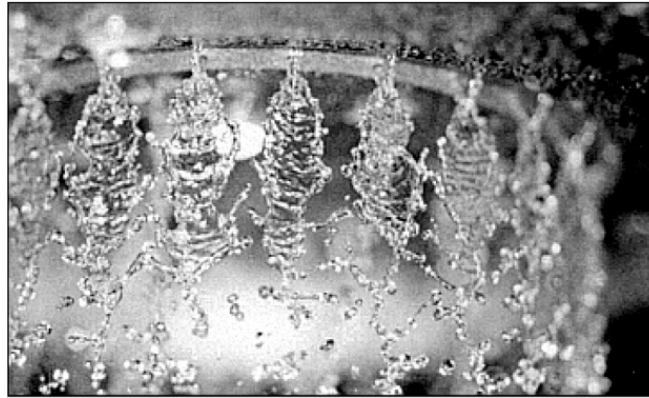
$$We = \frac{\rho u^2 d}{\sigma} \tag{1}$$

Fig. 1. Impacting jets in the combustion chamber of the gas generator of an industrial propulsion engine from SNECMA (see also [1]).

The sheet radial extension is either solely dependent on *We*, or depends both on *We* and on the ratio of the liquid to ambient gas densities $\alpha = \rho_a/\rho$. The transition occurs for [8]

$$We = \mathcal{O}(\alpha^{-1/2}) \tag{2}$$

Below this limit, the sheet is smooth, and above, it sustains a shear, flag-like Kelvin–Helmholtz type of instability resulting from a global coupling between the liquid and its environment, usually a gas phase (see Squire (1953) [9], also [10–13] and Fig. 2). The onset of this instability alters dramatically the fragmentation process of the sheet, leading to comparatively much finer drops whose ultimate formation process is still under debate [14].

The study of soap films has been conducted by a different school of thought, not immediately motivated by particular applications, and its experimental facet has really emerged with Ranz [16] and Mysels [17,18]. Much effort has been paid at understanding the different kind of waves a film can sustain [19] and at the hole opening dynamics, when the film is punctured. At the hole rim, surface tension forces are no longer balanced, driving a flow from the hole edge to the bulk of the film which is limited by liquid inertia. The long standing question of the exact value of the opening velocity was solved by Taylor [6] and Culick [20], after attempts by Dupré [21] and Rayleigh [22] using a flawed energy conservation approach.

Yet, if the question of the rim receding velocity is settled, the question of its stability is still unsolved. However, its ultimate destabilization is an obvious feature of the overall opening dynamics, as illustrated in Fig. 3, but its analysis has to date resisted a convincing representation, despite several attempts in related contexts aiming at describing a capillary instability of a Plateau–Rayleigh type of a thick cylindrical-like rim attached to a thin sheet.

We report in this article on novel observations suggesting that the phenomenology of flapping sheets from fan spray nozzles familiar in agricultural sewage or combustion chambers is, as surprising as it may be, the same as that of spontaneously bursting soap films.

2. Edge receding velocity

When an initially quiet liquid film is punctured, the equilibrium of surface tension forces in the plane of the film is broken. If the hole diameter is big enough (i.e. larger than the film thickness typically), the hole opens and the liquid constitutive of the film is collected in a growing rim at the border of the hole (Fig. 4).

Disregarding the details of the rim shape and assuming that it is sufficiently compact so that its center of mass can be confused with its edge, the opening dynamics of the hole derives from global mass and momentum conservations applied to the rim, following the classical description of Taylor (1959) [6] and Culick (1960) [20]. For a film of uniform thickness h, uniform surface tension σ, and liquid density ρ, these amount to

$$\frac{\mathrm{d}}{\mathrm{d}t}\big(x(t)\dot{x}(t)\big) = \frac{2\sigma}{\rho h} \tag{3}$$

where $x(t)$ stands for the location of the center of mass of the rim and for $x(0) = 0$ (i.e. with a vanishingly small initial mass). The factor 2 in Eq. (3) comes from the two sides of the film. The solution of (3) is a *constant* velocity
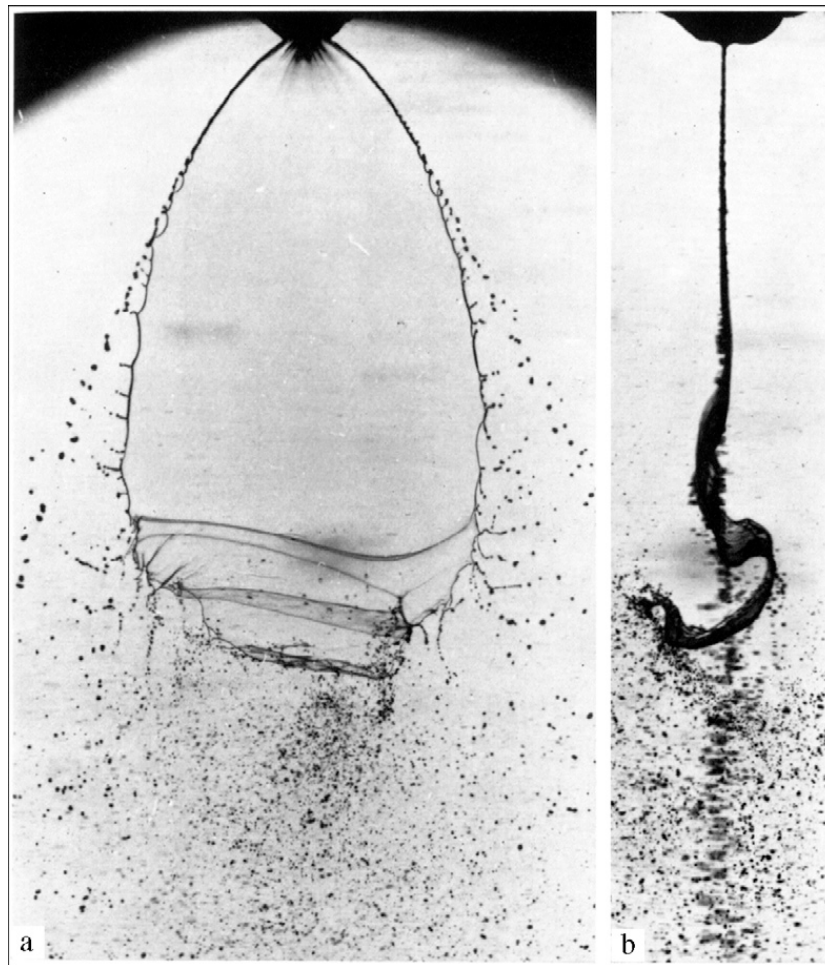
Fig. 2. Liquid sheet issuing from a fan spray nozzle ((a) front and (b) side views, reproduced from [15]) showing the flag instability characteristic of liquid sheets moving rapidly with respect to their environment (see also [8]).

$$V = \frac{x(t)}{t} = \sqrt{\frac{2\sigma}{\rho h}} \tag{4}$$

known as the *Taylor–Culick* velocity expressing a balance between a constant force 2σ applied to a growing mass $\rho h x(t)$. The relevance of this result for soap films was confirmed experimentally by McEntee and Mysels (1969) [17]. That velocity is considerable for thin films. For instance, a typical soap film is $h = 1$ μm thick and recedes at $V = 6$ m/s.

The time it takes for the rim to accelerate up to its limit speed V is of the order of several times h/V. In the experiment shown in Fig. 4, the film was pierced by a spark of typical size $10h$. As seen in Fig. 4, the rim has traveled by much more than 10 times the film thickness h while remaining smooth, so that this short acceleration period is actually negligible if one is interested in the later stages of the rim destabilization.

3. The picture *with* surfactant

The simple sketch recalled above consisting of a concentrated mass at the rim pulled by a constant force is relevant for pure liquids like water sheets [6,23]. However, when it is formed from a soap solution, the layer of surfactant at its surface confers to the sheet an original surface rheology which modifies drastically the rim shape, without altering the global mass and momentum balances, and therefore the limit receding velocity. The reason is that local surface tension on the film depends on the local surfactant concentration Γ [24]. Precisely, σ decreases typically when Γ increases: a compressed area of the film $\Gamma' > \Gamma$, as those close to the rim will thus have a tension σ' smaller that
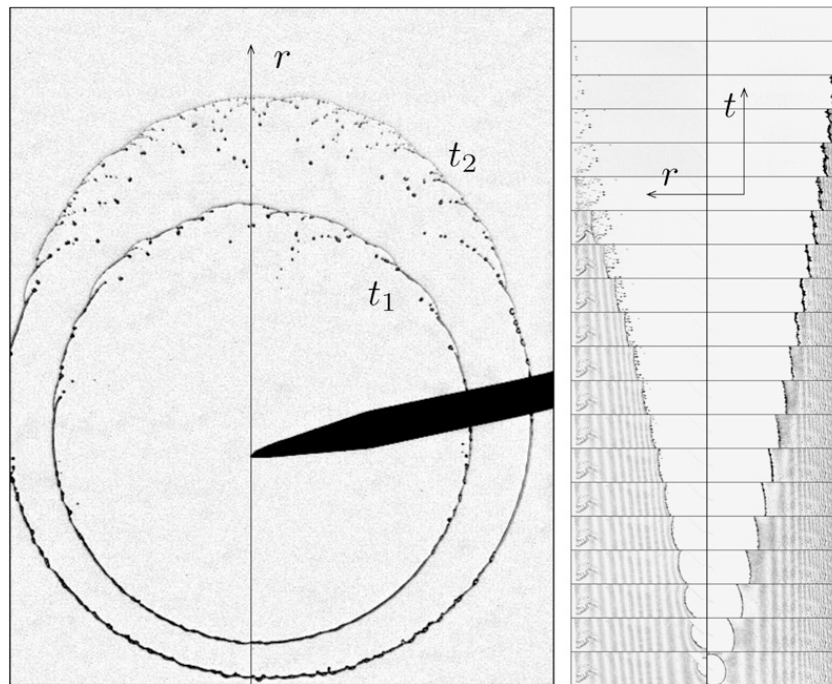
Fig. 3. Opening dynamics of a soap film standing vertically and punctured by a sharp object. Left: Front view showing how the hole has opened at two consecutive instants of time t_1 and t_2, and how its rim progressively destabilizes. Right: Space time diagrams in the vertical direction towards the top and the bottom of the film evidencing acceleration of the rim towards the thinner regions of the film, and deceleration towards the thicker regions.
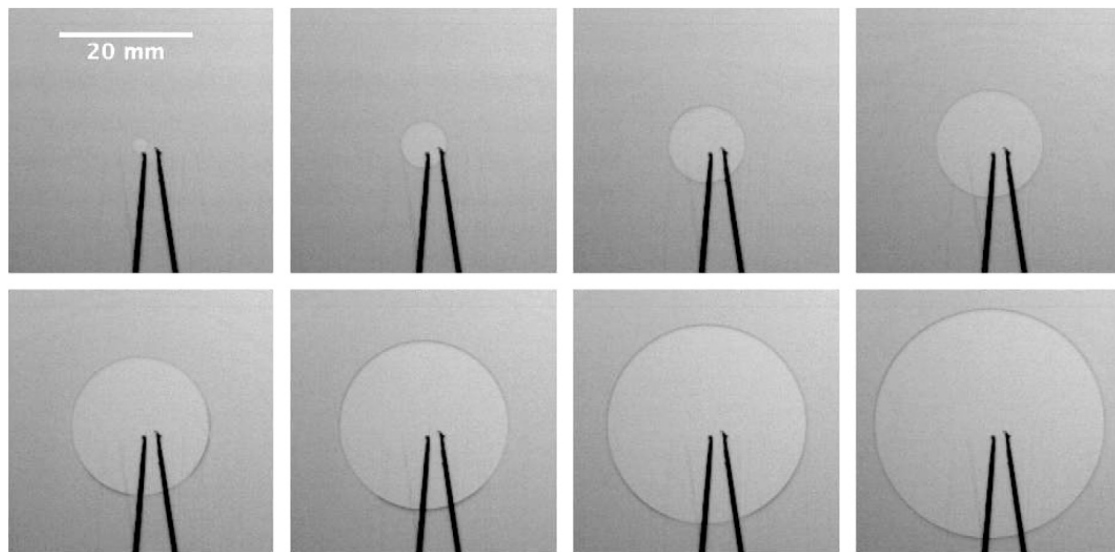

Fig. 4. Early stage of the opening of a soap film. Images are sampled every 200 µs.

those far from the rim σ given by the equilibrium concentration Γ. A net force $\sigma - \sigma'$ thus appears from the rim recession, which contributes to the liquid rearrangement in the rim.

The result is an *extended rim*, with fluid particles moving far ahead from the hole edge and a marching rim shape. The phenomenon can be quantified by an interferometric method as described below.

3.1. Experiments and observations

A solution of commercial surfactant (Dreft by Procter & Gamble, a mixture of non-ionic and anionic molecules) is diluted in tap water. The concentration in surfactant is always larger than the critical micelle concentration, a
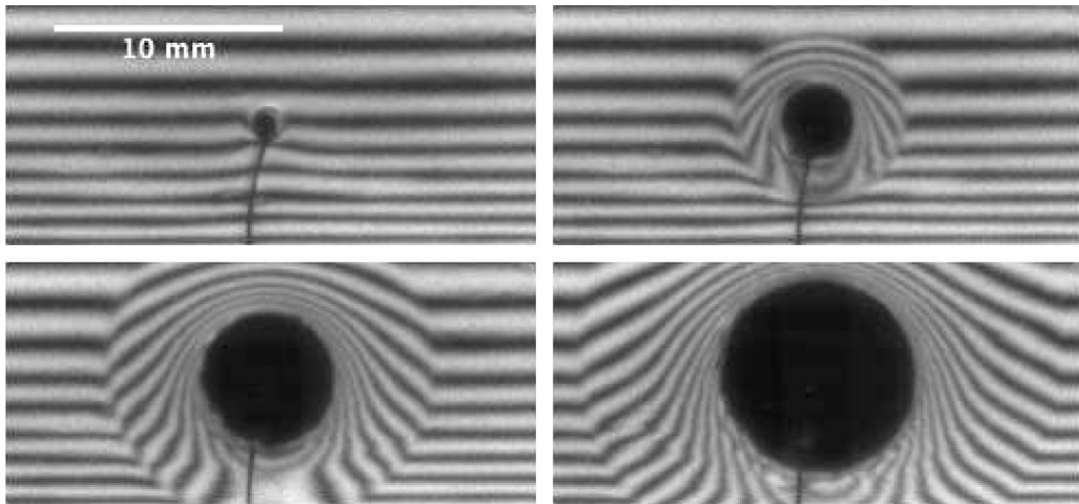
Fig. 5. Evidence of the aureole surrounding an opening hole in a flat soap film. The initial parallel interference fringes are perpendicular to gravity. Images are sampled every 320 µs.

concentration above which aggregates (micelles) form and surface tension saturates. This ensure surface tension of the solution to have at saturation value $\sigma = 32 \times 10^{-3}$ N/m.

A 10×20 cm^2 aluminum frame is immersed into the solution and is pulled out slowly to form a flat rectangular soap film standing vertically in the gravity field. For the whole experiment, the frame supporting the film is kept in a vapor saturated atmosphere to prevent liquid evaporation.

The film is lit by a diffuse monochromatic source coming from a mono mode argon laser operating at wavelength $\lambda_l = 488$ nm. The beam is scattered by a lens to form a spot on a diffuser. Fringes are observed by reflexion over the film (see Fig. 5 and also [25]). They are either constructive or destructive interference fringes between rays that reflect on the upper film interface and those that are reflected by the rear interface. The difference of path length between the reflected rays depend on the local thickness h and thus a fringe traces locations of constant thickness. For a film lit under a weak incidence angle, the difference of film thickness between two consecutive black fringes is [26]

$$\Delta h = \frac{\lambda_l}{2n \cos r} \simeq \frac{\lambda_l}{2n} \tag{5}$$

where n is the refraction index of water and r is the refraction angle. The distance between two consecutive fringes is thus a direct measure of the local thickness gradient.

A sequence of the opening of such a soap film is shown in Fig. 5 taken with a Photron APX digital fast camera operating at 25 000 frames/s. The initial interference pattern in Fig. 5 shows that h is uniform along horizontal lines but varies with altitude (i.e. the direction where gravity points). Higher locations correspond to weaker gradients. This "Eiffel tower"-like thickness profile is a consequence of liquid drainage under gravity. The corresponding equilibrating surface tension gradient is however much weaker that the one generated by the hole opening, as Fig. 5 demonstrates also.

The film is punctured by an electric arc generated by a potential difference of several kVolts applied to two electrodes facing each other, one above and one behind the film. The hole nucleated by the arc grows with time, keeping a disk shape characteristic of an isotropic opening velocity V. Around the disk, a region of typical radial extent $L(t) \sim Vt$ develops, where the fringes pattern is modified. McEntee and Mysels (1969) [17] observed this region for the first time and called it the "aureole", a crystal-clear term to depict Fig. 5.

A way to extract information from these movies is to focus on the horizontal segment starting at the puncture point which corresponds to an initially thick-uniform film section. A spatio-temporal diagram of the brightness pattern along this segment is shown on Fig. 6. On this diagram, horizontal distances from the left-hand border represent the spatial distance r from the piercing point, whereas vertical distances from the top border represent the time elapsed since the piercing instant.
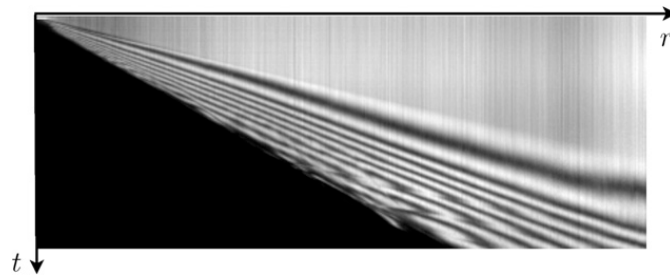
Fig. 6. Spatio-temporal diagram showing the evolution of an initially uniform film section. The top left corner is the piercing point. The width of the picture represents 4.5 cm and its height corresponds to 6.5 ms.
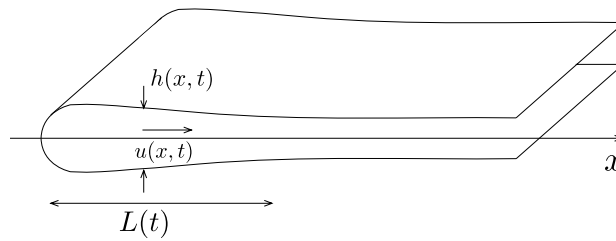

Fig. 7. Sketch of the rim shape, or aureole. The width $L(t)$ is proportional to the distance traveled by the edge Vt.

It is immediately clear on this (r, t) diagram that the trajectory of any iso-thickness path is straight. This means that their velocities in the laboratory frame of reference are constant in time. Each of those velocities is in addition easy to measure with a good accuracy.

From the disk opening velocity V given by Eq. (4), the value of the initial thickness h is measured. Since interference fringes provide an information on the relative thickness between different portions of the film only, this absolute thickness measurement is mandatory to reconstruct the thickness profile of the whole film from the complete interference pattern.

3.2. Driving forces and rim shape

The aureole has its origin in the surface tension gradients generated by the hole motion itself that surfactant solutions authorize, in contrast with pure liquids for which surface tension is a constant (albeit thermal effects which are absent here).

We will discuss the equations governing the base state of thickness and liquid velocity fields in the aureole in the one dimensional approximation (corresponding to the case of a rupture of the film along a straight line instead at in a point). This does not change the ingredients of the problem, but makes its exposition simpler.

At constant thickness, the problem presents a translation invariance along the rim direction (Fig. 7). That invariance is eventually broken by the development of the rim instability, which we will consider next. The physical scales of the problem are: $h \sim 1\ \mu m$ (thickness), $L > 1\ mm$ (radial extent), $\rho = 10^3\ kg\,m^{-3}$ (liquid density), $\sigma = 32 \times 10^{-3}\ N\,m^{-1}$ (surface tension of the soap solution at equilibrium), $\mu = 10^{-3}\ N\,m^{-2}\ s$ (liquid viscosity).

The starting point is that thickness gradients in the aureole, $h_x \sim h/L < 10^{-3}$ are weak. This legitimates a slender slope description, where averaged thickness $h(x, t)$ and velocity $u(x, t)$ profiles are seek for, with no explicit representation of the motion in the (small) direction perpendicular to the film (see e.g. [27]). For an incompressible liquid, the conservations laws are

$$h_t + (uh)_x = 0 \qquad\qquad (6)$$

$$\rho h(u_t + uu_x) = f \qquad\qquad (7)$$

where f stands for the resultant forces (by unit of length) applying to a film section. An order of magnitude estimate of the different forces involved in f is as follows:

- Surface tension itself (independently of its gradient) contributes through Laplace law (κ is the interface curvature) as

$$\sigma(h\kappa)_x \sim \frac{1}{2}\sigma(hh_{xx})_x \sim \frac{1}{2}\left(\frac{h}{L}\right)^3 \frac{\sigma}{h} \tag{8}$$

- Viscous effects, assuming a Newtonian viscous response, integrated over the film thickness arise through a Trouton term [27]

$$4\mu(hu_x)_x \sim \frac{8h_0}{L^2}\frac{\mu}{\sqrt{2\sigma\rho h_0}}\sigma \sim 8Oh\left(\frac{h}{L}\right)^2 \frac{\sigma}{h} \tag{9}$$

where the Ohnesorge number $Oh = \mu/(\sqrt{2\sigma\rho h})$ is the ratio of surface tension forces to viscous dissipation forces and is of the order of 10^{-1} to 1 in the present case.

- Lastly, the stress resulting from the gradient of surfactant concentration, sometimes referred to as a Marangoni stress gives a contribution

$$\left(\frac{2\sigma}{\sqrt{1+h_x^2}}\right)_x \sim 2\left(\frac{h}{L}\right)\frac{\sigma}{h} \tag{10}$$

With $h/L < 10^{-3}$, it is clear that the last term dominates over the others. If one moreover assumes that surfactant molecules have no time to reorganize at the interface and are advected in a passive way with the fluid (see e.g. [28]), one has $d\ln\Gamma = d\ln h$. This provides a new set of equations in place of (6) and (7)

$$h_t + uh_x = -hu_x \tag{11}$$

$$u_t + uu_x = \frac{2\sigma_x}{\rho h} \tag{12}$$

with

$$\frac{2\sigma_x}{\rho h} = -\left(\frac{E}{\rho h^3}\right)hh_x \tag{13}$$

where E, possibly depending on h, is a Marangoni elasticity module

$$E = -2\frac{d\sigma}{d\ln\Gamma} = -2\frac{d\sigma}{d\ln h} \tag{14}$$

The origin of this surface elasticity is that surface tension σ decreases as the surface concentration of surfactant Γ increases. Rim recession induces a contraction of area in the film plane, and thus a local decrease of σ, hence the net force in (12) which appears to be, owing to the order of magnitude estimates made above, the dominant driving force. The system of Eqs. (11) and (12) was solved by Frankel and Mysels (1969) [18] using the methods of characteristics.

The first result is that for unidimensional receding aureoles, solutions depend on the law $\sigma(h)$ only. They have the self-similar form

$$\begin{cases} h(x,t) = h\mathcal{F}\left(\dfrac{x}{Vt}\right) \\ u(x,t) = V\mathcal{G}\left(\dfrac{x}{Vt}\right) \end{cases} \tag{15}$$

where $\mathcal{F}$ and $\mathcal{G}$ are functions depending on the details of the $\sigma(h)$ dependence. Although technically more complex in the axi-symmetrical coordinates relevant to a punctual piercing with radial expansion along r, the solutions are also self similar in r/Vt, consistently with the measurements shown in the next section.

The second result is that the rim receding velocity V is almost not affected by the dependence $\sigma(h)$, which nevertheless is responsible for the existence of an aureole. This was checked by McEntee and Mysels [17] since their empirical confirmation of the Taylor–Culick prediction for V was carried out on soap films.
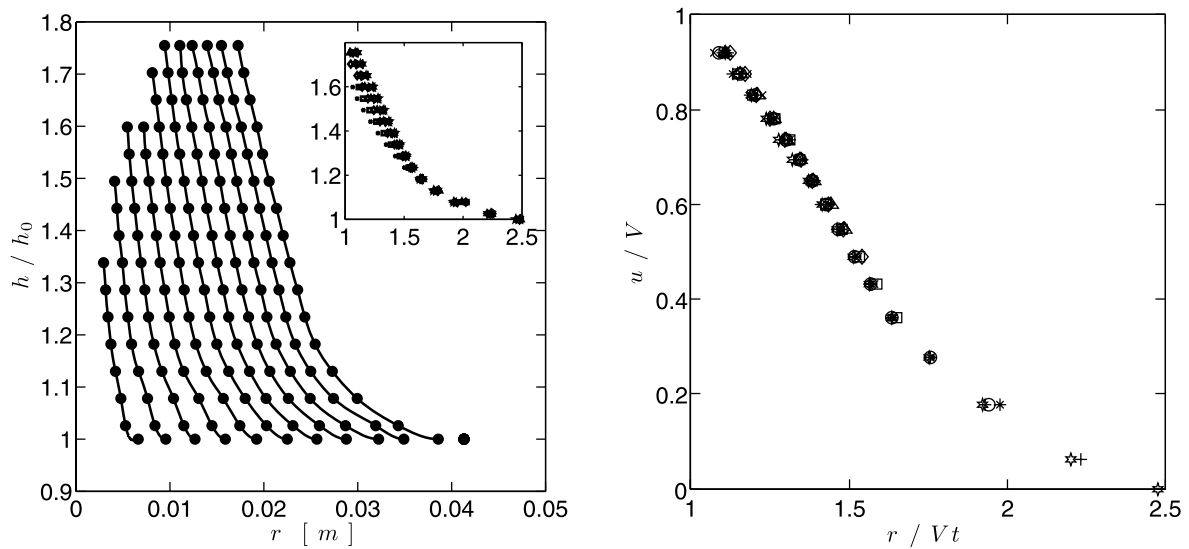
Fig. 8. Left: Thickness profiles of the aureole at successive instants of the bursting sampled every 320 µs. Dots represent measurements and lines are meant to guide the eyes. Insert: the same profiles plotted versus r/Vt. Right: Liquid velocity profiles of the aureole at successive instants of the bursting versus radius r scaled by the current edge position Vt sampled every 320 µs.

3.3. Measurements

Radial thickness profiles of the aureole $h(r, t)$ were computed from fringes patterns at distinct times t and are plotted in Fig. 8. They exhibit the expected similar shape (hence giving a direct measurement of the function $\mathcal{F}$) as well as a saturation of the maximal thickness we were able to measure close to the rim edge at $h(0) \approx 2h$. This may be indicative of the maximal compression ratio the sheet is able to sustain.

The liquid velocity can also be reconstructed, using mass conservation in the axi-symmetrical case

$$u(r, t) = \frac{1}{hr} \int_r^{r_0} \frac{\partial h}{\partial t} r \, dr \tag{16}$$

where r_0 is a radial location far from the rim, in the unperturbed region of the film. The obtained velocity profiles are shown in Fig. 8. They are plotted versus r scaled by the current edge position Vt. Their superposition on a same curve is a direct proof of their self similarity, defining experimentally the function $\mathcal{G}$ introduced in Eq. (15). From the film edge moving at V to the limit of the aureole moving 2.5 times faster, the liquid velocity u has decreased from V to 0, since the unperturbed portion of the film is not, by definition, set into motion yet.

4. Flapping

The existence of an extended rim, or aureole, genuine to soap films as described above has a direct consequence on their stability. Precisely, the liquid is set into motion far ahead from the rim edge, and thus sustains a shear with the surrounding medium for an ever longer radial distance, of the order of $L(t)$ as time elapses. This shear, as it is known since Squire (1953) [9], potentially leads to an instability. This remark, illustrated below is, to our knowledge, new in the context of soap films.

That shear instability, of a standard Kelvin–Helmholtz type, sustains two different modes, a varicose mode in which both interfaces move in phase opposition and a sinuous mode (flapping) in which they move in phase. The latter is the most amplified [8].

A fundamental difference with the pure Kelvin–Helmholtz instability between two infinite phases is related to the finite thickness h of the film, sandwiched between two lighter infinite phases, since instability can only develop in that case above a threshold given by

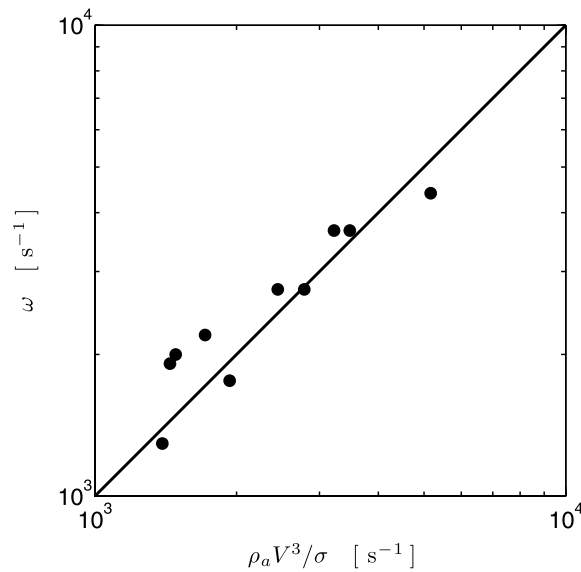$$We = \frac{\rho u(x, t)^2 h(x, t)}{\sigma(h)} > 2 \tag{17}$$

Fig. 9. Flapping pulsation ω versus $\rho_a V^3/\sigma$.

where $u(x,t)$ is the velocity difference between the film and the outer light (in the present case air) still phase. This threshold simply expresses that the local velocity difference $u(x,t)$ should be at least equal to $\sqrt{2\sigma(h)/\rho h}$ for instability to occur.

Obviously, there is a region close to the rim edge where this condition is likely to be satisfied. There, the film thickness is larger than h and the local surface tension $\sigma(h)$ is lower than σ, while $u(x,t)$ is of the order of V (see Fig. 8). This region defines the unstable zone, in the sense of Squire according to the criterion in Eq. (17).

Experiments clearly show that the edge of a receding soap film flaps (see Fig. 10) in a way reminiscent of the well known flapping sheets of uniform velocity, and surface tension (see Fig. 2). Two flapping waves also appear in Fig. 6 as a perturbation of the self similar pattern. They birth in the unperturbed region of the film, and their amplitude peaks at the edge. Assuming, for simplicity, an infinite, uniform film of thickness h in relative motion at velocity $u(x,t) \approx V$ with an air environment of density ρ_a, the most amplified wavelength and the pulsation scales are [8]

$$
\begin{cases}
\lambda \sim \dfrac{\sigma}{\rho_a V^2} \sim \dfrac{\rho}{\rho_a} h \\[2mm]
\omega \sim \dfrac{V}{\lambda} \sim \dfrac{\rho_a V^3}{\sigma}
\end{cases}
\tag{18}
$$

Measurements of the flapping pulsation in air under standard temperature and pressure conditions for which $\rho_a = 1.2 \text{ kg m}^{-3}$ are shown in Fig. 9. The pulsation (or flapping) frequency follows the anticipated trend in Eq. (18) in law, and in absolute value, thus supporting the scenario rooted on a shear instability we have proposed.

5. Rim indentations

When observed over a longer time period than the one in Fig. 4, a bursting soap film will be seen to suddenly destabilize. Indentations pointing toward the center of the hole appear on the formerly smooth edge, becoming the ejection sites of liquid ligaments which later pinch off to form the final spray. A sequence of this phenomenon is presented on Fig. 10. The phenomenon has been known for a while, and the flapping mechanism provides a clue to understanding it. The scenario for the formation of the indentations transverse to the rim derives from the "wavy corridor" mechanism imagined by Bremond et al. [14] for the destabilization of undulating Savart sheets. The wavy pattern consecutive of the flapping instability propagates at a group velocity proportional to V on the film. A fluid particle in the flapping region thus experiences transient accelerations perpendicular to the film plane (whose intensity is $\gamma = a\omega^2$ for a flapping amplitude a) as the wave propagates. This, in turn, initiates a *Rayleigh–Taylor* instability of the film which causes film thickness modulations at a transverse wavelength $\lambda_\perp$, precursors of the rim indentations visible in Fig. 10. The full mechanism is thus a succession of two destabilizations of the film. The first shear instability
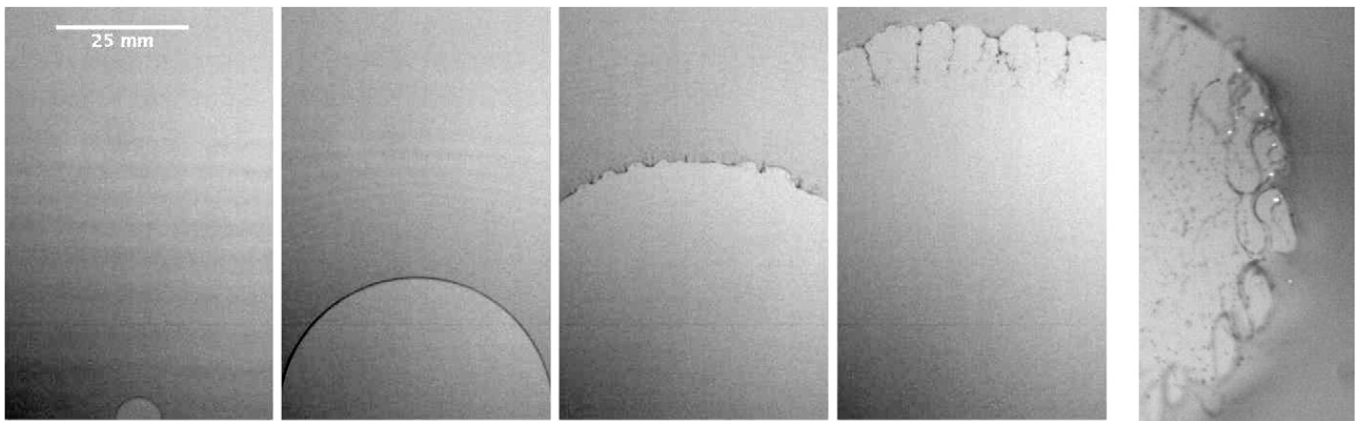
Fig. 10. Left: Evidence of the rim destabilization in a soap film. Images are sampled every 6.7 ms. Right: Snapshot emphasizing on indentations. Note the arabesques, ligaments detaching from the rim as they flap like a whip.
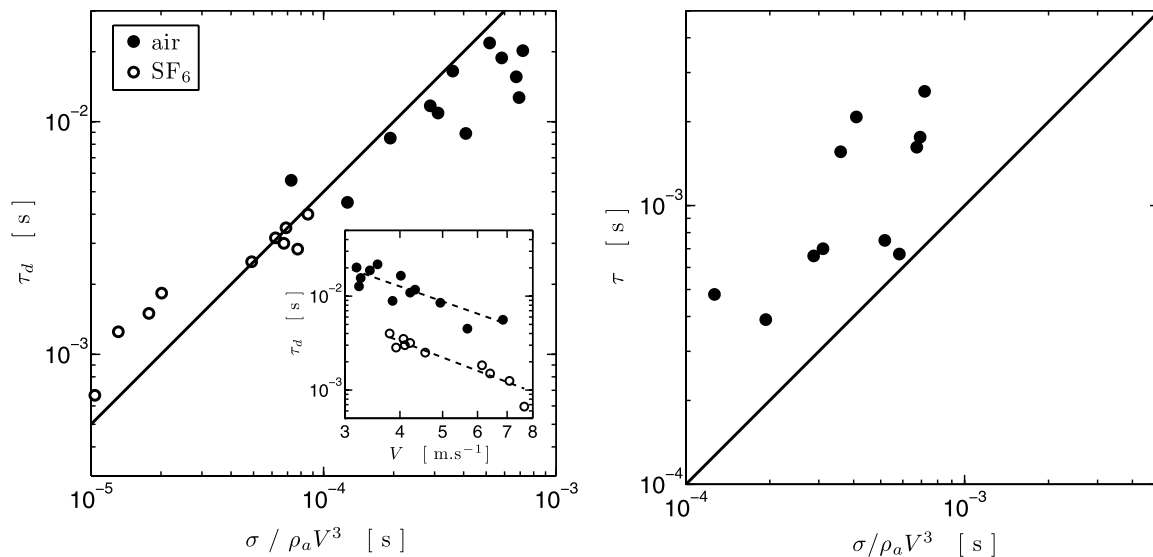

Fig. 11. Left: Delay time τ_d before destabilization occurs versus $\sigma/\rho_a V^3$. Insert: the same data plotted versus V. Right: Characteristic indentations growth time τ versus $\sigma/\rho_a V^3$.

breaks the symmetry with respect to the film median plane, and a second inertial instability of the undulating substrate breaks the axial-symmetry by forming indentations.

Let s be the growth rate of the transverse, Rayleigh–Taylor instability for a given flapping pulsation, wave amplitude, and film thickness. The transverse indentation will onset as soon as the permanence time of the acceleration perpendicular to the film ω^{-1} will be at least equal to the instability development time s^{-1}. The transverse instability criterion is thus [8,14]

$$\omega = s \tag{19}$$

also providing an estimate for the *delay time* before the onset of indentations τ_d, and for the time of growth of the indentation amplitude τ which are both expected to scale like ω^{-1} i.e.

$$\tau_d \sim \tau \sim \omega^{-1} \tag{20}$$

These expectations have been tested experimentally using two different surrounding atmospheres in order to check the role of the density ratio ρ_a/ρ. We bursted soap films both into air and into hexafluorosulfur (SF$_6$), whose density under standard conditions is 5 times that of air.

Films receding at a same given velocity were seen to develop indentations after a shorter delay τ_d when bursting into SF$_6$ than when bursting into air, as expected according to Eq. (18). This fundamental observation demonstrates
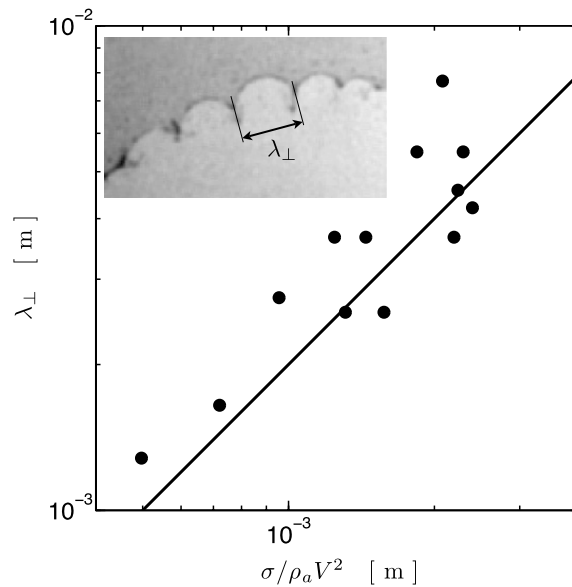
Fig. 12. Indentations transverse wavelength $\lambda_\perp$ as defined in the insert, versus $\sigma/\rho_a V^2$.

that the rim instability is directly influenced by the outer medium. Measurements are presented on Fig. 11. Both τ_d and τ are increasing functions of $\sigma/\rho_a V^3$, with however a somewhat weaker trend than the one anticipated from Eq. (18).

The transverse Rayleigh–Taylor instability of the rim is rooted in the transient accelerations experienced by the liquid as it flows through the primary wavy pattern of the sheet. Let γ be the intensity of this acceleration. The cut-off wavenumber of the instability is $k_c = \sqrt{\rho\gamma/\sigma}$. If $k_c h \gg 1$, the instability growth rate is $s \sim \sqrt{\gamma/\lambda_\perp}$ with $\lambda_\perp \sim \sqrt{\sigma/\rho\gamma}$. In the opposite limit i.e. when $k_c h \ll 1$, the growth rate s as well as $\lambda_\perp$ now depend on the film thickness as [14]

$$s = \sqrt{\frac{\gamma}{\lambda_\perp}} \sim \sqrt{\frac{\rho\gamma^2 h}{\sigma}} \quad \text{and} \quad \lambda_\perp \sim \left(k_c^2 h\right)^{-1} \tag{21}$$

This limit is by far the relevant one here (see Figs. 10 and 12) so that $\lambda_\perp^2 h \sim \sigma/\rho s^2$ providing, with $s \sim \omega \sim \rho_a V^3/\sigma$ and $h \sim \sigma/\rho V^2$

$$\lambda_\perp \sim \lambda \tag{22}$$

The primary undulation and secondary indentation patterns have alike lengthscales, representing a strong dependence of $\lambda_\perp$ on V indeed observed experimentally in trend, and absolute values as seen in Fig. 12.

6. Conclusion

The set of observations reported here have demonstrated the direct coupling between the destabilization of a receding rim in a soap film, and the medium in which it bursts. That observation is original in the context of soap films and is a consequence of a flapping instability of the extended aureole that forms as a punctured hole opens. That flapping induces a secondary Rayleigh–Taylor type of instability of the rim, explaining the birth of its transverse indentations. The phenomenon is surprisingly analogue to the well known flapping regime of liquid sheets, and has been analyzed along the same lines.

The flapping mechanism, discovered and documented here, also answers the unsolved question of the *ejection angle* of the drops released by the rim. De Gennes (1996) [29] has proposed that the drops are ejected at an angle with respect to the film plane because the rim edge is a stagnation point the drops avoid while keeping their kinetic energy. The present vision rather suggests that drops are ejected by ligaments which flap like whips (this is obvious in Fig. 10), spreading out the drops out of the film plane.

The structure of the spray and resulting drop size distribution is left for future work.

References

[1] N. Bremond, E. Villermaux, Atomization by jet impact, J. Fluid Mech. 549 (2006) 273–306.

[2] F. Savart, Mémoire sur le choc de deux veines liquides animées de mouvements directement opposés, Ann. Chim. 55 (1833) 257–310.

[3] F. Savart, Mémoire sur le choc d'une veine liquide lancée sur un plan circulaire, Ann. Chim. 54 (1833) 56–87.

[4] F. Savart, Suite du mémoire sur le choc d'une veine liquide lancée sur un plan circulaire, Ann. Chim. 54 (1833) 113–145.

[5] G.I. Taylor, The dynamics of thin sheets of fluid. ii. Waves on fluid sheets, Proc. R. Soc. London 253 (1959) 296–312.

[6] G.I. Taylor, The dynamics of thin sheets of fluid. iii. Disintegration of fluid sheets, Proc. R. Soc. London 253 (1959) 313–321.

[7] J.C.P. Huang, The break-up of axisymmetric liquid sheets, J. Fluid Mech. 43 (1970) 305–319.

[8] E. Villermaux, C. Clanet, Life of a flapping liquid sheet, J. Fluid Mech. 462 (2002) 341–363.

[9] H.B. Squire, Investigation of the stability of a moving liquid film, British J. Appl. Phys. 4 (1953) 167–169.

[10] J.L. York, H.E. Stubbs, M.R. Tek, The mechanism of disintegration of liquid sheets, Trans. ASME (1953) 1279–1286.

[11] W.W. Hagerty, J.F. Shea, A study of the stability of plane fluid sheets, J. Appl. Mech. 22 (1955) 509–514.

[12] G.I. Taylor, Formation of thin flat sheets of water, Proc. R. Soc. London 259 (1960) 1–17.

[13] S.P. Lin, Breakup of Liquid Sheets and Jets, Cambridge University Press, 2003.

[14] N. Bremond, C. Clanet, E. Villermaux, Atomization of undulated liquid sheets, J. Fluid Mech. 585 (2007) 421–456.

[15] G.D. Crapper, N. Dombrowski, W.P. Jepson, G.A.D. Pyott, A note on the growth of Kelvin–Helmholtz waves on thin liquid sheets, J. Fluid Mech. 57 (1973) 671–672.

[16] W.E. Ranz, Some experiments on the dynamics of liquid films, J. Appl. Phys. 30 (1959) 1950.

[17] W.R. McEntee, K.J. Mysels, The bursting of soap films. i. An experimental study, J. Phys. Chem. 73 (1969) 3018–3028.

[18] S. Frankel, K.J. Mysels, The bursting of soap films. ii. Theoretical considerations, J. Phys. Chem. 73 (1969) 3028–3038.

[19] E.H. Lucassen-Reynders, J. Lucassen, Properties of capillary waves, Adv. Colloid Interface Sci. 2 (1969) 347–395.

[20] F.E.C. Culick, Comments on a ruptured soap film, J. Appl. Phys. 31 (1960) 1128.

[21] A. Dupré, Théorie mécanique de la chaleur, Ann. Chim. Phys. 11 (1868) 194.

[22] L. Rayleigh, Some applications of photography, Nature XLIV (1891) 249–254.

[23] C. Clanet, E. Villermaux, Life of a smooth liquid sheet, J. Fluid Mech. 462 (2002) 307–340.

[24] R. Fowler, E.A. Guggenheim, Statistical Thermodynamics, Cambridge University Press, UK, 1952.

[25] N.Y. Liang, C.K. Chan, H.J. Choi, Dynamics of the formation of an aureole in the bursting of soap films, Phys. Rev. E 54 (4) (1996) R3117–R3120.

[26] C. Isenberg, The Science of Soap Films and Soap Bubbles, Dover, 1992.

[27] J. Eggers, E. Villermaux, Physics of liquid jets, Rep. Prog. Phys. 71 (2008) 036601.

[28] P. Marmottant, E. Villermaux, C. Clanet, Transient surface tension of an expanding liquid sheet, J. Colloid Interface 230 (2000) 29–40.

[29] P.G. de Gennes, Mechanics of soft interfaces, Faraday Discuss. 104 (1996) 1–8.